Two-dimensional and emission-tunable : an unusual perovskite constructed from lindqvist-type [Pb6Br19]7- nanoclusters

Li, Xinxiong; Ha Do, T. Thu; Águila, Andrés Granados Del; Huang, Yinjuan; Chen, Wangqiao; Li, Yongxin; Ganguly, Rakesh; Morris, Samuel; Xiong, Qihua; Li, Dong-Sheng; Zhang, Qichun

2018

Li, X., Ha Do, T. T., Águila, A. G. D., Huang, Y., Chen, W., Li, Y., . . . Zhang, Q. (2018). Two-dimensional and emission-tunable : an unusual perovskite constructed from lindqvist-type [Pb6Br19]7- nanoclusters. Inorganic Chemistry, 57(22), 14035–14038. doi:10.1021/acs.inorgchem.8b02535

https://hdl.handle.net/10356/142685

https://doi.org/10.1021/acs.inorgchem.8b02535

Two-Dimensional and Emission-Tunable: An Unusual Perovskite Constructed From Lindqvist-Type $[Pb_6Br_{19}]^{7-}$ Nanoclusters

Xinxiong Li,[†Δ] T. Thu Ha Do,[‡Δ] A. Granados del Águila,[‡] Yinjuan Huang,[†] Wangqiao Chen,[†] Yongxin Li,[§] Rakesh Ganguly,[§] Samuel Morris,[†] Qihua Xiong,[‡*] Dong-sheng Li,[¥] Qichun Zhang[†*]

[†]School of Materials Science and Engineering, Nanyang Technological University, 50 Nanyang Avenue, 639798, Singapore (Singapore)

[‡]Division of Physics and Applied Physics, School of Physical and Mathematics Science, Nanyang Technological University, 21 Nanyang Link, 637371, Singapore (Singapore)

[§]Division of Chemistry and Biological Chemistry, School of Physical and Mathematics Science, Nanyang Technological University, 637371, Singapore (Singapore)

[¥]College of Material and Chemical Engineering, Hubei Provincial Collaborative Innovation Center for New Energy Microgrid, Key Laboratory of Inorganic Nonmetallic Crystalline and Energy Conversion Materials, China Three Gorges University, Yichang 443002, China

Supporting Information Placeholder

ABSTRACT: Preparing low-dimensional perovskite materials with novel building units is highly desirable because such materials have already been demonstrated to show unusual physical properties. In this report, we firstly reported a new and unusual two-dimensional perovskite framework $[B(HIm)_4]_4Pb_{13}Br_{38}$ (**1**), constructed from novel Lindqvist-type $[Pb_6Br_{19}]^{7-}$ nanoclusters. The as-prepared material shows good water-resistance and chemical/heat stability. More importantly, **1** has been proved to exhibit temperature-/excitation-wavelength-dependent emission. The possible mechanism has been provided.

As an emerging class of high-performance semiconductors, organic-inorganic hybrid metal-halide perovskites have been demonstrated to show unique optical, electrical and mechanical properties.[1] Among all reported organic-inorganic hybrid metal-halide perovskite materials, 3-dimensional (3-D) structures have been widely used as active elements in solar cells[2] with the power conversion efficiency more than 20%.[2b] However, 3-D perovskite materials have some intrinsic drawbacks including heat stability, moisture sensitivity and light stability, which have become the major challenge for their applications in large area.[3] In order to address these problems, scientists found that low dimensional structure is a solution. Among all low-dimensional structures, two-dimensional (2-D) metal-halide perovskites have received huge attentions due to their superior thermal stability, chemical stability, and moisture-resistance coupled with high performance.[4] Moreover, comparing to 3-D perovskites, 2-D perovskites also offer more opportunities to tune their structures for modulating their physical properties including band gap, charge carrier dynamics and so on.[5] Thus, it is not surprising to witness recent surging researches in novel 2-D metal-halide perovskite materials and their applications.[6]

Generally, 2-D metal-halide perovskites can be realized by slicing the 3-D perovskites along different crystallographic planes *via* interleaving large organic spacer cations such as protonated aliphatic or aromatic ammonium/diammonium species, and the as-prepared 2-D perovskites with corner-sharing metal-halide octahedra can have the layer thickness up to five.[7] However, in the crystal lattices of these 2-D perovskites, the metal-halide octahedra still maintain the corner-sharing linking mode similar to the parent 3-D perovskites, which might provide less chances to adjust the structures and compositions of the inorganic 2-D layers. As we know, the structures, compositions and the layer thickness of the 2-D inorganic layer have great effect on their band gap, exciton absorption energy, and the photoelectric performance.[8] Thus, it is extremely important to construct new 2-D perovskites with new building units and their connecting modes.

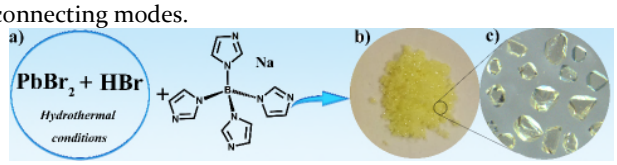

Figure 1 a) The synthetic route of **1**. b-c) View of the crystals of **1** by naked eyes and under an optical microscope.

In this research, we introduced a rigid multi-imidazole specie tetrakis(imidazolyl)borate $[B(Im)_4]^-$ (Im = imidazole, Figure 1a) as a structure-directing agent to explore novel 2-D perovskite materials, basically taking account of the following reasons: 1) $[B(Im)_4]^-$ is a good precursor to generate spacer cations when it is protonated; 2) the high-charge quantity of the protonated $[B(HIm)_4]^{3+}$ may induce halogen anions and Pb^{2+} ions to form novel metal-halide clusters *in situ*; and 3) protonated $[B(HIm)_4]^{3+}$ cations can serve as structure-

directing templates to direct the further assembly of *in situ* formed clusters into novel extended architectures. Here, we report an unprecedented 2-D hybrid perovskite $[B(HIm)_4]_4Pb_{13}Br_{38}$ (**1**). Single crystal X-ray diffraction (SCXRD) analysis reveals that the inorganic 2-D layer structure of **1** is constructed from Lindqvist-type $[Pb_6Br_{19}]^{7-}$ nanoclusters linked by $[PbBr_6]^{4-}$ octahedra, which is different from that in generally-reported 2-D perovskites. It is noteworthy that the Lindqvist-type metal-halide clusters are quite rare in metal-halide chemistry. To the best of our knowledge, **1** is the first 2-D perovskite material based on Lindqvist-type metal-halide nanoclusters.

The as-prepared **1** was obtained as light-yellow crystals by reacting $PbBr_2$, HBr and $NaB(Im)_4$ under hydrothermal condition (Figure 1). SCXRD structural study indicates that **1** belongs to trigonal space group $P3_121$ (Table S1), and its asymmetric unit is composed of seven unique Pb^{2+} ions, nineteen Br^- anions and two protonated $[B(HIm)_4]^{3+}$ cations (Figure S1). All Pb^{2+} ions adopt a little distorted octahedral coordination geometry. One of the most interesting structural features in **1** is the presence of an uncommon Lindqvist-type $[Pb_6Br_{19}]^{7-}$ cluster (Figure 2a-b). The lindqvist-type clusters are a type of classical polyoxometalate structures composed of MO_6 (M = V, Mo, W, Nb, Ta) octahedral with formula of $[M_6O_{19}]^{2-/8-}$, and their common structural characteristic is that six M atoms are joined together through a μ_6-O bridging atom to generate a $[\mu_6\text{-}OM_6]$ octahedron (Figure S2).[9] In the $[Pb_6Br_{19}]^{7-}$ cluster, six Pb^{2+} ions are connected together through one μ_6-Br^- anion, generating a $[\mu_6\text{-}BrPb_6]$ core. The core is further stabilized by twelve μ_2-Br^- bridges and six terminal Br^- ligands, leading to a Lindqvist-type cluster. The bond distances for Pb-Br_c, Pb-Br_b and Pb-Br_t (Br_c = μ_6-Br^-; Br_b = μ_2-Br^-; Br_t = terminal Br^- ligand) are within the limit of 3.141 ~ 3.391, 2.868 ~ 3.224, and 2.782 ~ 3.079 Å, respectively, which is comparable with those in the previously-reported bromoplumbates.[10] The whole size of the $[Pb_6Br_{19}]^{7-}$ cluster is about 1.23×1.23×1.23 nm^3, which is much larger than the Lindqvist-type metal-oxygen clusters in polyoxometalate chemistry (Figure S2), probably due to the larger Pb-Br bond distances than the M-O (M = Mo, W, V, Nb, Ta) bond lengths ($d_{M\text{-}O}$ = 1.582 ~ 2.446 Å). As far as we know, such a Lindqvist-type $[Pb_6Br_{19}]^{7-}$ cluster is very scarce,[11] although various haloplumbate clusters have been reported so far.[12]

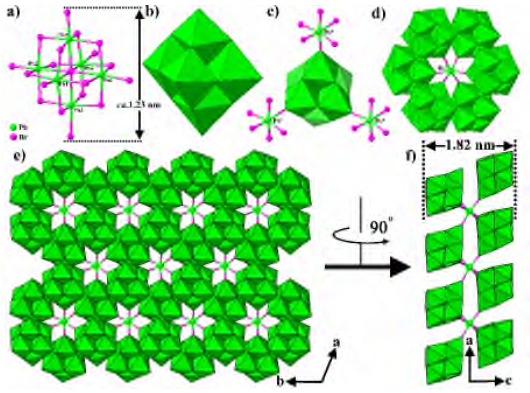

Figure 2 a-b) Structure of the $[Pb_6Br_{19}]^{7-}$ cluster. c-d) The coordination environment of $[Pb_6Br_{19}]^{7-}$ cluster and Pb7 ion, respectively. e-f) Top and side view of the 2-D layer structure.

The second fascinating structural feature in **1** is the further assembly of $[Pb_6Br_{19}]^{7-}$ clusters. As depicted in Figure 2c, each $[Pb_6Br_{19}]^{7-}$ cluster connects to three Pb^{2+} (Pb7) ions through sharing three mutually adjacent vertexes of the $[Pb_6Br_{19}]^{7-}$ cluster, forming a three-connected node. While, each Pb7 ion connects six $[Pb_6Br_{19}]^{7-}$ clusters through its six vertexes, resulting in a six-connected fragment (Figure 2d). The linkage of $[Pb_6Br_{19}]^{7-}$ clusters and Pb7 ions finally generates a 2-D layer structure with the thickness of ~ 1.82 nm (Figure 2e-f). As far as we know, such a Lindqvist-type cluster-based 2-D layer structure has never been reported in metal-halide chemistry. From the polyhedral point of view, the thickness of the 2-D inorganic layer can also be considered as five times of a recumbent lead-halide polyhedron (Figure S3). So far, the record of inorganic layer thickness based on corner-sharing metal-halide polyhedra in the reported 2-D lead-halide perovskites with well-defined crystal structures is five.[7] Therefore, **1** also represents a new member of 2-D lead-halide perovskites which contains inorganic layers with record polyhedral thickness.

Most noteworthy is the role of protonated $[B(HIm)_4]^{3+}$ cations, which is the third interesting structural feature in **1**. All $[B(HIm)_4]^{3+}$ cations not only act as charge-balancing cations for the anionic inorganic 2-D layers, but also serve as templates to direct the construction of the final structure. As depicted in Figure S4, each $[B(HIm)_4]^{3+}$ cation locates at the central vacancy generated by three surrounded $[Pb_6Br_{19}]^{7-}$ clusters, which is much different from those protonated aliphatic or aromatic ammonium/diammonium spacer cations in conventional 2-D perovskites usually locate at the interspace between two inorganic layers.[7] The tetrahedral $[B(HIm)_4]^{3+}$ cation matches well with the size and the shape of the vacancy, which further testifies the template effect of $[B(HIm)_4]^{3+}$ cations during the structure formation course. In addition to the electrostatic interactions between the $[B(HIm)_4]^{3+}$ cations and the inorganic 2-D layers, there are abundant N-H···Br, C-H···Br hydrogen bonds in the structure (Table S2), which may be helpful for enhancing the structure stability. Finally, the 2-D layers adopt an A-B-C-A stacking mode in the *c* axis, leading to the formation of the bulk crystals (Figure S5).

The as-prepared **1** is very stable in water, air, and ordinary organic solvents such as acetone, ethanol, methanol and so on (Figure S6). The good consistency between powder X-ray diffraction (PXRD) pattern for the as-prepared sample and the simulated one based on SXRD result indicates the phase purity of **1** (Figure S7). Thermogravimetric analysis of **1** displays no weight loss in the temperature from 30 to 300 °C (Figure S8), showing that **1** has a very good thermal stability. Variable-temperature PXRD measurement (Figure S7) further confirms that **1** can keep its crystallinity up to 300 °C. The peak around 350 °C in DSC curve (Figure S8) corresponds to the heat release caused by the skeleton collapse and the combustion of organic component.

Optical property of **1** has been investigated by steady-state ultraviolet-visible (UV-Vis) and photoluminescence (PL) spectroscopy. In the case of semi-infinite medium, where multi-reflection and interference effects can be safely neglected, the absorbance (A) directly correlates with transmittance (T_r) and reflectance (R) as $A = 1 - T_r - R$ (Figure S9). While T_r and R are taken from the UV-Vis experiments, the absorbance profile can be derived and presented as a function of photon energy, by the blue curve in Figure 3a. From low- to high-energy side, the absorption is almost null at energies below ~ 2.5 eV, then increases dramatically, and eventually saturates at energies above 3.0 eV. The absorption

onset determines the optical bandgap (E_g), which is defined as the minimum energy required for an interband transition from the highest-occupied-molecular-orbital (HOMO) to the lowest-unoccupied-molecular-orbital (LUMO) state. Furthermore, the sharp increment resembles the absorption edges of direct-bandgap semiconductors (e.g., GaAs, CdTe), and differs from those of indirect-bandgap semiconductors (e.g., Si, Ge).[13] Therefore, our result suggests the direct nature of the bandgap transition in **1**. Quantitatively, the optical bandgap can be estimated from the typical Tauc plot for a direct-bandgap semiconductor (Figure S10) as $E_g \approx 2.7$ eV, which is comparable to II-VI semiconductors (CdS,[14] ZnSe[15]), lead-halide perovskite[16] and organic semiconductors.[17]

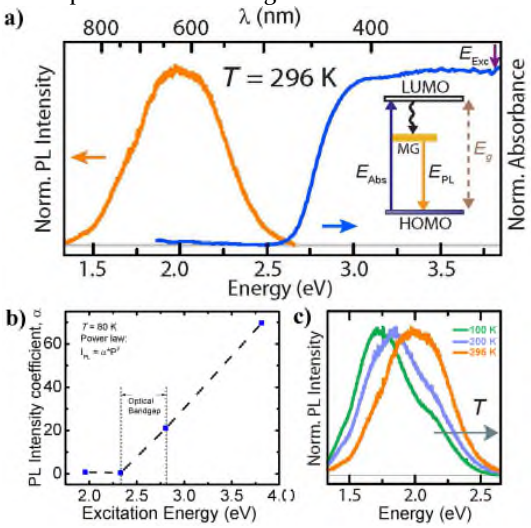

Figure 3. a) Normalized optical spectra, absorption (blue) and photoluminescence (orange). In PL measurements, excitation energy of E_{Exc} ~ 3.82 eV (λ_{Exc} = 325 nm) was used (purple arrow). Inset: simplified energy scheme describing the emission mechanism. b) Photoluminescence excitation (PLE) profile that agrees with the absorption spectrum in a). c) PL spectra taken at selected temperatures.

In addition, the crystal of **1** exhibits strong photoluminescence signal (Figure 3a, orange curve) when using excitation energy of 3.82 eV (λ_{Exc} = 325 nm). The emission peak is centered at $E_{PL} \approx 2.0$ eV, which is about 0.7 eV smaller than the optical bandgap. Such large energy deviation between E_g and E_{PL} is unlikely to stem from the interaction between the photoexcited carriers and vibrational (phonon) modes of the crystal lattice, which normally causes a much smaller energy shift of about 0.1 eV.[18] Hence, we attribute the origin of the PL emission of compound **1** to mid-gap (MG) states. An electron, originally residing at the HOMO state, can be excited to LUMO state by absorbing a high-energy photon (*i.e.* $E_{Abs} \geq E_g$). As a result of fast relaxation processes to the MG states, a PL signal arises at the energy E_{PL} (inset in Figure 3a). Under external stimuli, such as temperature or pressure, the luminescence from these MG states may vary accordingly with the bandgap. We conducted photoluminescence excitation (PLE) experiment at T = 80 K, where the PL spectrum is monitored by varying the laser wavelengths and varying powers at each wavelength. The PL intensity coefficient α is extracted from the power law $I = \alpha * P^{\beta}$ (Figure S11) and plotted as a function of excitation energy (Figure 3b). In the case of fast relaxation, PLE profile should reflect the absorptivity of the crystal. The PL intensity is weak when the excitation energy is smaller than the bandgap (E_{Exc} = 2.33 eV) and even at the PL spectral position (E_{Exc} = 1.96 eV). On the other hand, the emission is very strong by using above-bandgap excitation energies (E_{Exc} = 3.82 eV, 2.81 eV). The good agreement between the PLE (Figure 3b) and the absorption (Figure 3a) profile, therefore, strongly supports for the afore-proposed emission mechanism. The response of the PL emission (λ_{Exc} = 325 nm) to temperature is depicted in Figure 3c. The PL spectra at selected temperatures are normalized for comparison. Intriguingly, the PL spectral peak shifts to higher energies (blue-shift) as the temperature increases. This temperature-induced blue-shift is opposite to conventional semiconductors[19] and is the fingerprint of lead halide semiconductors with perovskite lattices.[20] Moreover, the PL peak shift in response to temperature is reversible. The PL quantum yield of **1** measured at ambient temperature is about 3.4%, which is comparable with benzylammonium lead bromide perovskite (3.8%).[21] Time-resolved photoluminescence was measured at ambient temperature and the decay curve fitting is obtained with two decay channels with τ_1 = 0.5 ns and τ_2 = 2.8 ns (Figure S12).

In conclusion, an unprecedented 2-D perovskite, which shows several distinct structural charactersitics, has been successfully prepared. The deliberate choice of tetrakis(imidazolyl)borate as a structure-directing agent is key for the generation of the 2-D material. The optical investigation indicates that **1** is a direct-bandgap semiconductor with bandgap of about 2.7 eV. Importantly, the strong broadband emission of **1**, covering the visible-near infrared region of the electromagnetic spectrum, promotes itself as potential candidate for solar photovoltaic, sensing applications. Furthermore, the massive energy shift from near-ultraviolet absorption to visible-near infrared emission can optimize the reabsorption efficiency that is advantageous for a luminescence light concentrator. This finding will not only enrich the structural multiplicity of 2-D perovskite materials, but also present a new outlook for the development of novel haloplumbates with unique photoelectronic properties.

ASSOCIATED CONTENT

Supporting Information

Experimental details, crystallographic data for **1**, additional structural figures, characterizations. This material is available free of charge via the internet at http://pubs.acs.org.

AUTHOR INFORMATION

Corresponding Author

*Email: qihua@ntu.edu.sg
*Email: qczhang@ntu.edu.sg

Author Contributions

ΔThese authors contributed equally.

Notes

The authors declare no competing financial interest.

ACKNOWLEDGMENT

Q. Zhang acknowledges financial support from AcRF Tier 1 (RG 2/17, RG 111/17, RG 8/16, RG 114/16) and Tier 2 (MOE 2017-T2-1-021), Singapore. Q. Xiong gratefully acknowledges the financial support from Singapore Ministry of Education via AcRF Tier 1 grants (RG 194/17 and RG 113/16).

REFERENCES

(1) a) Stoumpos, C. C.; Kanatzidis, M. G. The Renaissance of Halide Perovskites and Their Evolution as Emerging Semiconductors. *Acc. Chem. Res.* **2015**, *48*, 2791-2802. b) Zhu, J. C.; Di, Q.; Zhao, X. X.; Wu, X. T.; Fan, X.; Li, Q.; Song, W. D.; Quan, Z. W. Facile Method for the Controllable Synthesis of CsxPbyBrz-Based Perovskites. *Inorg. Chem.* **2018**, *57*, 6206-6209. c) Wang, N.; Liu, W.; Zhang, Q. Perovskite-Based Nanocrystals: Synthesis and Applications Beyond Solar Cells. *Small Methods*, **2018**, *2*, 1700380. d) Zhang, Y. L.; Ding, R.; Li, S. N.; Jiang, Y. C.; Hu, M. C.; Zhai, Q. G. Ionothermal Design of Crystalline Halogeno(cyano)cuprate Family: Structure Diversity, Solid-State Luminescence, and Photocatalytic Performance. *Inorg. Chem.*, **2017**, *56*, 7161-7174. e) Hu, F.; Zhai, Q. G.; Li, S. N.; Jiang, Y. C.; Hu, M. C. Ionothermal synthesis of a new (4,12)-connected heterometallic iodoplumbate with $[Pb_4(OH)_4]$ cubane as joint points of the helices. *CrystEngComm*, **2011**, *13*, 414-417. f) Wang, M. S.; Guo, G. C. Inorganic–organic hybrid white light phosphors. *Chem. Commun.* **2016**, *52*, 13194-13204.

(2) a) Wang, N.; Zhao, K.; Ding, T.; Liu, W.; Ahmed, A. S.; Wang, Z.; Tian, M.; Sun, X. W.; Zhang, Q. Improving Interfacial Charge Recombination in Planar Heterojunction Perovskite Photovoltaics with Small Molecule as Electron Transport Layer. *Adv. Energy Mater.* **2017**, *7*, 1700522. b)Tsai, H.; Asadpour, R.; Blancon, J. C.; Stoumpos, C. C.; Durand, O.; Strzalka, J. W.; Chen, B.; Verduzco, R.; Ajayan, P. M.; Tretiak, S.; Even, J.; Alam, M. A.; Kanatzidis, M. G.; Nie, W.; Mohite, A. D. Light-induced lattice expansion leads to high-efficiency perovskite solar cells. *Science* **2018**, *360*, 67-70. c) Wang, M. S.; Guo, G. C.; Chen, W. T.; Xu, G.; Zhou, W. W.; Wu, K. J.; Huang, J. S. A White-Light-Emitting Borate-Based Inorganic-Organic Hybrid Open Framework. *Angew. Chem. Int. Ed.* **2007**, *46*, 3909-3911.

(3) a) Domanski, K.; Alharbi, E. A.; Hagfeldt, A.; Gratzel, M.; Tress, W. Systematic investigation of the impact of operation conditions on the degradation behaviour of perovskite solar cells. *Nat. Energy* **2018**, *3*, 61-67. b) Kaltzoglou, A.; Stoumpos, C. C.; Kontos, A. G.; Manolis, G. K.; Papadopoulos, K.; Papadokostaki, K. G.; Psycharis, V.; Tang, C. C.; Jung, Y.; Walsh, A.; Kanatzidis, M. G.; Falaras, P. Trimethylsulfonium Lead Triiodide: An Air-Stable Hybrid Halide Perovskite. *Inorg. Chem.* **2017**, *56*, 6302-6309. c) Gu, P. Y.; Wang, N.; Wang, C.; Zhou, Y.; Long, G.; Tian, M.; Chen, W.; Sun, X. W.; Kanatzidis, M. G.; Zhang, Q. Pushing up the efficiency of planar perovskite solar cells to 18.2% with organic small molecular as electron transport layer. *J. Mater. Chem. A.* **2017**, *5*, 7339-7344.

(4) a) Saparov, B.; Mitzi, D. B. Organic–Inorganic Perovskites: Structural Versatility for Functional Materials Design. *Chem. Rev.* **2016**, *116*, 4558-4596. b) Hautzinger, M. P.; Dai, J.; Ji, Y. J.; Fu, Y. P.; Chen, J.; Guzei, I. A.; Wright, J. C.; Li, Y. Y.; Jin, S. Two-Dimensional Lead Halide Perovskites Templated by a Conjugated Asymmetric Diammonium. *Inorg. Chem.* **2017**, *56*, 14991-14998.

(5) Soe, C. M. M.; Stoumpos, C. C.; Kepenekian, M.; Traore, B.; Tsai, H.; Nie, W.; Wang, B. H.; Katan, C.; Seshadri, R.; Mohite, A. D.; Even, J.; Marks, T. J.; Kanatzidis, M. G. New Type of 2D Perovskites with Alternating Cations in the Interlayer Space, $(C(NH_2)_3)(CH_3NH_3)_nPb_nI_{3n+1}$: Structure, Properties, and Photovoltaic Performance. *J. Am. Chem. Soc.* **2017**, *139*, 16297-16309.

(6) Shi, E. Z.; Gao, Y.; Akriti, B. P.; Coffey, A. H.; Dou, L. T. Two-dimensional halide perovskite nanomaterials and heterostructures. *Chem. Soc. Rev.* **2018**, *47*, 6046-6072.

(7) Stoumpos, C. C.; Cao, D. H.; Clark, D. J.; Young, J. J.; Rondinelli, M.; Jang, J. I.; Hupp, J. T.; Kanatzidis, M. G. Ruddlesden–Popper Hybrid Lead Iodide Perovskite 2D Homologous Semiconductors. *Chem. Mater.* **2016**, *28*, 2852-2867.

(8) Mao, L.; Wu, Y.; Stoumpos, C. C.; Wasielewski, M. R.; Kanatzidis, M. G. White-Light Emission and Structural Distortion in New Corrugated Two-Dimensional Lead Bromide Perovskites. *J. Am. Chem. Soc.* **2017**, *139*, 5210-5215.

(9) a) Li, X. X.; Zhang, L. J.; Cui, C. Y.; Wang, R. H.; Yang, G. Y. Designed Construction of Cluster Organic Frameworks from Lindqvist-type Polyoxovanadate Cluster. *Inorg. Chem.* **2018**, *57*, 10323-10330. b) Fullmer, L. B.; Mansergh, R. H.; Zakharov, L. N.; Keszler, D. A.; Nyman, M. Nb_2O_5 and Ta_2O_5 Thin Films from Polyoxometalate Precursors: A Single Proton Makes a Difference. *Cryst. Growth Des.* **2015**, *15*, 3885-3892.

(10) a) Lin, H.; Zhou, C.; Tian, Y.; Besara, T.; Neu, J.; Siegrist, T.; Zhou, Y.; Bullock, J.; Schanze, K. S.; Ming, W.; Du, M. H.; Ma, B. Bulk assembly of organic metal halide nanotubes. *Chem. Sci.* **2017**, *8*, 8400-8404. b) Tong, Y. B.; Ren, L. T.; Duan, H. B.; Liu, J. L.; Ren, X. M. An amphidynamic inorganic-organic hybrid crystal of bromoplumbate with 1,5-bis(1-methylimidazolium)pentane exhibiting multi-functionality of a dielectric anomaly and temperature-dependent dual band emissions. *Dalton Trans.* **2015**, *44*, 17850-17858. c) Sun, C.; Wang, M. S.; Li, P. X.; Guo, G. C. Conductance Switch of a Bromoplumbate Bistable Semiconductor by Electron-Transfer Thermochromism. *Angew. Chem. Int. Ed.* **2017**, *56*, 554-558.

(11) Sun, C.; Du, M. X.; Xu, J. G.; Mao, F. F.; Wang, M. S.; Guo, G. C. A nanowire array with two types of bromoplumbate chains and high anisotropic conductance. *Dalton Trans.* **2018**, *47*, 1023-1026.

(12) a) Wu, L. M.; Wu, X. T.; Chen, L. Structural Overview and Structure-Property Relationships of Iodoplumbate and Iodobismuthate. *Coord. Chem. Rev.* **2009**, *253*, 2787-2804. b) Wang, G. E.; Xu, G.; Liu, B. W.; Wang, M. S.; Yao, M. S.; Guo, G. C. Semiconductive Nanotube Array Constructed from Giant $[Pb^{II}_{18}I_{54}(I_2)_9]$ Wheel Clusters. *Angew. Chem. Int. Ed.* **2016**, *55*, 514-518.

(13) Fox. M., Optical Properties of Solids. New York: Oxford University Press, **2010**.

(14) a) Kouser, S.; Lingampalli, S. R.; Chithaiah, P.; Roy, A.; Saha, S.; Waghmare, U. V.; Rao, C. N. R. Extraordinary Changes in the Electronic Structure and Properties of CdS and ZnS by Anionic Substitution: Cosubstitution of P and Cl in Place of S. *Angew Chem Int Ed.* **2015**, *54*, 8149-8153. b) Chen, Z.; Luo, D.; Luo, X.; Kang, M.; Lin, Z. Two-dimensional assembly of tetrahedral chalcogenide clusters with tetrakis(imidazolyl)borate ligands. *Dalton Trans.*, **2012**, *41*, 3942-3944.

(15) Al-Kuhaili, M. F.; Kayani, A.; Durrani, S. M. A.; Bakhtiari, I. A.; Haider, M. B. Band Gap Engineering of Zinc Selenide Thin Films Through Alloying with Cadmium Telluride. *ACS Appl. Mater. Interfaces*, **2013**, *5*, 5366-5372.

(16) a) Saba, M.; Quochi, F.; Mura, A.; Bongiovanni, G. Excited State Properties of Hybrid Perovskites. *Acc. Chem. Res.* **2016**, *49*,166-173. b) Xiang S. C.; Zhang, Y. F.; Wu, A. Q.; Cai, L. Z.; Guo, G. C.; Huang, J. S. A New Type of Hybrid Magnetic Semiconductor Based upon Polymeric Iodoplumbate and Metal-Organic Complexes as Templates. *Inorg. Chem.* **2006**, *45*, 1972-1977. c) Zhang, J. J.; Guo, G. C.; Xu Gang, Fu, M. L.; Zou, J. P.; Huang, J. S. $[(H_2en)_7(C_2O_4)_2]_n(Pb_4I_{18})_n{\cdot}4nH_2O$, a New Type of Perovskite Co-templated by Both Organic Cations and Anions. *Inorg. Chem.* **2006**, *45*, 10028-10030. d) Wang, G. E.; Xu, G.; Wang, M. S.; Cai, L. Z.; Li, W. H.; Guo, G. C. Semiconductive 3-D haloplumbate framework hybrids with high color rendering index white-light emission. *Chem. Sci.* **2015**, *6*, 7222-7226. e) Sun, C.; Xu, G.; Jiang, X. M.; Wang, G. E.; Guo, P. Y.; Wang, M. S.; Guo, G. C. Design Strategy for Improving Optical and Electrical Properties and Stability of Lead-Halide Semiconductors. *J. Am. Chem. Soc.*, **2018**, *140*, 2805-2811.

(17) Costa, J. C. S.; Taveira, J. S. R.; Carlos, F. R. A. C.; Mendes, L. A.; Santos, M. N. B. F. L. Optical band gaps of organic semiconductor materials. *Opt. Mater.* **2016**, *58*, 51-60.

(18) Ullrich, B.; Ariza, F. D.; Bhowmick, M. Intrinsic photoluminescence Stokes shift in semiconductors demonstrated by thin-film CdS formed with pulsed-laser deposition. *Thin Solid Films.* **2014**, *558*, 24-26.

(19) Zilli, A.; Luca, M. D.; Tedeschi, D. H.; Fonseka, A.; Miriametro, A.; Tan, H. H.; Jagadish, C.; Capizzi, M.; Polimeni, A. Temperature Dependence of Interband Transitions in Wurtzite InP Nanowires. *ACS Nano* **2015**, *9*, 4277-4287.

(20) Do, T. T. H.; Águila, A. G. D.; Cui, C.; Xing, J.; Ning, Z. J.; Xiong, Q. H. Optical study on intrinsic exciton states in high-quality $CH_3NH_3PbBr_3$ single crystals. *Phys. Rev. B*, **2017**, *96*, 075308.

(21) Kawano, N.; Koshimizu, M.;Sun, Y.; Yahaba, N.; Fujimoto, Y.; Yanagida, T.; Asai, K. Effects of Organic Moieties on Luminescence Properties of Organic-Inorganic Layered Perovskite-Type Compounds. *J. Phys. Chem. C*, **2014**, *118*, 9101-9106.

Table of Contents and Synopsis

Two-Dimensional and Emission-Tunable: An Unusual Perovskite Constructed From Lindqvist-Type $[Pb_6Br_{19}]^{7-}$ Nanoclusters

Xinxiong Li,[†Δ] T. Thu Ha Do,[‡Δ] A. Granados del Águila,[‡] Yinjuan Huang,[†] Wangqiao Chen,[†] Yongxin Li,[§] Rakesh Ganguly,[§] Samuel Morris,[†] Qihua Xiong,[‡*] Dong-sheng Li,[¥] Qichun Zhang[†*]

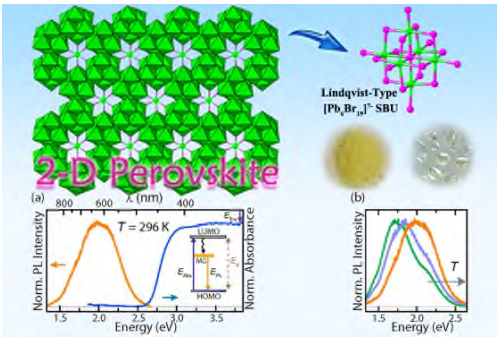

An unusual 2-dimensional perovskite constructed from rare Lindqvist-type $[Pb_6Br_{19}]^{7-}$ nanoclusters has been successfully prepared. The as-prepared 2-D material is a wide-gap semiconductor (~2.7 eV) and displays temperature-/excitation-wavelength-dependent emission.